Variational collocation on finite intervals

2007 J. Phys. A: Math. Theor. 40 13047

(http://iopscience.iop.org/1751-8121/40/43/013)

IOP Publishing Journal of Physics A: Mathematical and Theoretical

J. Phys. A: Math. Theor. **40** (2007) 13047–13062 doi:10.1088/1751-8113/40/43/013

Variational collocation on finite intervals

Paolo Amore[1], **Mayra Cervantes**[1] **and Francisco M Fernández**[2]

[1] Facultad de Ciencias, Universidad de Colima, Bernal Díaz del Castillo 340, Colima, Colima, Mexico
[2] INIFTA (Conicet, UNLP), Diag. 113 y 64 S/N, Sucursal 4, Casilla de Correo 16, 1900 La Plata, Argentina

E-mail: paolo@ucol.mx, mayradcv@ucol.mx and fernande@quimica.unlp.edu.ar

Received 20 February 2007, in final form 10 September 2007
Published 9 October 2007
Online at stacks.iop.org/JPhysA/40/13047

Abstract
In this paper, we study a set of functions, defined on an interval of finite width, which are orthogonal and which reduce to the sinc functions when the appropriate limit is taken. We show that these functions can be used within a variational approach to obtain accurate results for a variety of problems. We have applied them to the interpolation of functions on finite domains and to the solution of the Schrödinger equation, and we have compared the performance of the present approach with others.

PACS numbers: 03.30.+p, 03.65.−w

(Some figures in this article are in colour only in the electronic version)

1. Introduction

The main goal of this paper is to study the application of a set of orthogonal functions to the solution of a wide class of problems, such as function interpolation and the numerical solution of differential equations, including the Schrödinger equation. These functions, which are defined on a finite domain, have appeared in a number of works under different names: for example, Meyer calls them 'trigonometric interpolation functions' in [1], Schwartz relates them to a Fourier basis in [2], Baye and Heenen call them 'diffraction-like Lagrange functions' in [3], while they appear as 'psinc' in [4]. More recently Amore has referred to these functions as 'little sinc functions' (LSF) in [5], where they have been used to obtain an alternative representation for non-local operators and path integrals. In this paper, we will adopt this last convention. The relation of these functions to usual sinc functions is discussed in [6].

In recent years, Baye and collaborators have used these and other functions for the solution of the Schrödinger equation with several different potentials, and they have produced accurate numerical results both for the energies and wavefunctions [3, 7, 8]. Collocation methods based on ordinary sinc function have been applied in the literature to a large class of problems,

which include those mentioned above (see, for example, [9]), and they have been put on firm mathematical grounds [10]. Examples of applications of the sinc functions can be found in [11–16], among others. Recently, one of the authors has shown that the sinc collocation methods can be optimized by using a variational approach [17] based on the principle of minimal sensitivity (PMS) [18]. This optimization allows one to obtain the highest precision with a given number of grid points, and can be particularly valuable in problems that require intense numerical calculation.

In this paper, we wish to discuss the general properties of the LSF, their relation to sinc functions and we extend the variational results of [17] to these functions.

This paper is organized as follows. In section 2, we describe the general properties of the usual sinc functions, defined on the real line. In section 3, we derive an expression for the LSF and discuss their properties. In section 4, we solve the Schrödinger equation with two different potentials and compare numerical results obtained with the usual sinc functions and LSF. Finally, in section 5 we draw our conclusions.

2. Sinc functions

In what follows we outline some of the basic properties of the sinc functions, defined as

$$S_k(h,x) \equiv \frac{\sin(\pi(x-kh)/h)}{\pi(x-kh)/h}, \tag{1}$$

for every $k \in \mathbb{Z}$, uniform grid spacing h and $x \in \mathbb{R}$. The sinc function for a given value of the index k is peaked at $x_k = kh$, where it equals unity, and vanish at the other points $x_j = jh$, with $j \neq k$ and $j \in \mathbb{Z}$.

From the integral representation

$$S_k(h,x) = \frac{h}{2\pi}\int_{-\pi/h}^{+\pi/h} \mathrm{e}^{\pm \mathrm{i}(x-kh)t}\,\mathrm{d}t, \tag{2}$$

we easily derive the normalization factor

$$\mathcal{I}_1 \equiv \int_{-\infty}^{+\infty} S_k(h,x)\,\mathrm{d}x = h, \tag{3}$$

and the orthogonality property

$$\mathcal{I}_2 \equiv \int_{-\infty}^{+\infty} S_k(h,x)S_l(h,x)\,\mathrm{d}x = h\delta_{kl}. \tag{4}$$

It is worth noting that equation (2) defines a Dirac delta function in the limit $h \to 0$.

A function $f(z)$ analytic on a rectangular strip in $\mathbb{C}$ centred on the real axis can be approximated in terms of sinc functions as [10]

$$f(x) \approx \sum_{k=-\infty}^{+\infty} f(kh)S_k(h,x), \tag{5}$$

which together with the normalization factor can be used to approximate the definite integral

$$\int_{-\infty}^{+\infty} f(x)\,\mathrm{d}x \approx h\sum_{k=-\infty}^{\infty} f(kh). \tag{6}$$

It is not difficult to derive simple expressions of the derivatives of sinc functions in terms of the same sinc functions:

$$\frac{\mathrm{d}}{\mathrm{d}x}S_k(h,x) = \sum_{l=-\infty}^{\infty} c_{lk}^{(1)}S_k(h,x), \tag{7}$$

where

$$c_{kl}^{(1)} \equiv \int_{-\infty}^{+\infty} S_l(h,x)\frac{\mathrm{d}}{\mathrm{d}x}S_k(h,x)\,\mathrm{d}x = \begin{cases} 0 & \text{if} \quad k=l \\ \frac{1}{h}\frac{(-1)^{k-l}}{k-l} & \text{if} \quad k\neq l. \end{cases} \tag{8}$$

For the second derivative we have

$$\frac{\mathrm{d}^2}{\mathrm{d}x^2}S_k(h,x) = \sum_{l=-\infty}^{\infty} c_{lk}^{(2)} S_k(h,x), \tag{9}$$

where

$$c_{lk}^{(2)} \equiv \int_{-\infty}^{+\infty} S_l(h,x)\frac{\mathrm{d}^2}{\mathrm{d}x^2}S_k(h,x)\,\mathrm{d}x = \begin{cases} -\frac{\pi^2}{3h^2} & \text{if} \quad k=l \\ -\frac{2}{h^2}\frac{(-1)^{k-l}}{(k-l)^2} & \text{if} \quad k\neq l. \end{cases} \tag{10}$$

General expressions for higher order derivatives are also available [16]:

$$c_{lk}^{(2r)} \equiv \frac{(-1)^{l-k}}{h^{2r}(l-k)^{2r}}\sum_{k=0}^{r-1}(-1)^{k+1}\frac{2r!}{(2k+1)!}\pi^{2k}(l-k)^{2k} \tag{11}$$

$$c_{ll}^{(2r)} \equiv \left(\frac{\pi}{h}\right)^{2r}\frac{(-1)^r}{2r+1} \tag{12}$$

$$c_{lk}^{(2r+1)} \equiv \frac{(-1)^{l-k}}{h^{2r+1}(l-k)^{2r+1}}\sum_{k=0}^{r}(-1)^{k}\frac{(2r+1)!}{(2k+1)!}\pi^{2k}(l-k)^{2k} \tag{13}$$

$$c_{ll}^{(2r+1)} \equiv 0, \tag{14}$$

with $r = 1, 2, \ldots$.

3. Little sinc functions

We will now derive the set of LSF. We consider the orthonormal basis of the wavefunctions of a particle in a box with infinite walls located at $x = \pm L$:

$$\psi_n(x) = \frac{1}{\sqrt{L}}\sin\left(\frac{n\pi}{2L}(x+L)\right), \qquad n = 1, 2, 3, \ldots \tag{15}$$

and define

$$\begin{aligned}\overline{\delta}_N(x,y) &= C_N\sum_{n=1}^{N}\psi_n(x)\psi_n(y) \\ &= \frac{C_N}{4L}\left\{\frac{\sin\left(\frac{(2N+1)\pi(x-y)}{4L}\right)}{\sin\left(\frac{\pi(x-y)}{4L}\right)} - (-1)^N\frac{\cos\left(\frac{(2N+1)\pi(x+y)}{4L}\right)}{\cos\left(\frac{\pi(x+y)}{4L}\right)}\right\},\end{aligned} \tag{16}$$

where C_N is a constant to be specified below.

Because of the completeness of the basis $\{\psi_n(x)\}$ on $x \in [-L, +L]$ we have

$$\lim_{N\to\infty}\frac{\overline{\delta}_N(x,y)}{C_N} = \delta(x-y). \tag{17}$$

For reasons that will soon become clear, we set $C_N = \frac{2L}{N}$ and select even values of N. To simplify the notation $h \equiv 2L/N$ will denote the grid spacing, and $y_k \equiv \frac{2kL}{N} = kh$, with $k = -N/2+1, -N/2+2, \ldots, N/2-1$, the grid points.

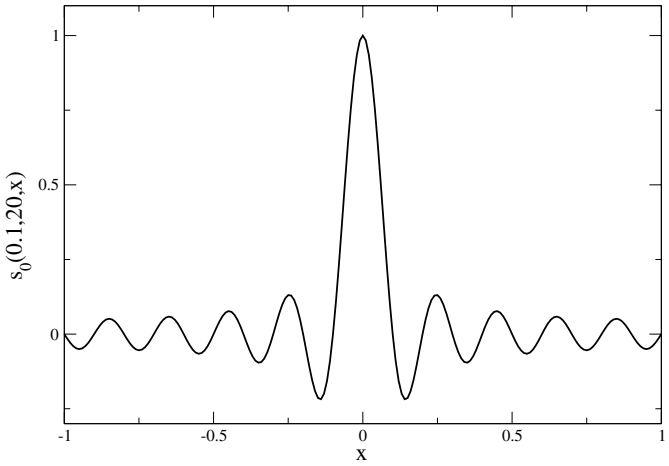

Figure 1. LSF for $N = 20$ and $k = 0$.

We then define a set of $(N-1)$ LSF

$$s_k(h,N,x) \equiv \frac{1}{2N}\left\{\frac{\sin\left(\left(1+\frac{1}{2N}\right)\frac{\pi}{h}(x-kh)\right)}{\sin\left(\frac{\pi}{2Nh}(x-kh)\right)} - \frac{\cos\left(\left(1+\frac{1}{2N}\right)\frac{\pi}{h}(x+kh)\right)}{\cos\left(\frac{\pi}{2Nh}(x+kh)\right)}\right\}. \tag{18}$$

By means of a well-known expression for the Chebyshev polynomial of the second kind [19] one can rewrite the LSF as[3]

$$s_k(h,N,x) \equiv \frac{1}{2N}\left\{U_{2N}\left[\cos\frac{\pi}{2Nh}(x-kh)\right] - U_{2N}\left[\sin\frac{\pi}{2Nh}(x+kh)\right]\right\} \tag{19}$$

Figure 1 shows one of these functions for $N = 20$.

It is not difficult to prove that the s_k are orthogonal

$$\int_{-L}^{L} s_k(h,N,x)s_j(h,N,x)\,\mathrm{d}x = h\delta_{kj}, \tag{20}$$

and satisfy,

$$s_k(h,N,y_j) = \delta_{kj}, \tag{21}$$

properties that are also shared by the sinc functions.

Therefore, it is not surprising that the LSF become the standard sinc functions when $N \to \infty$ and h is held constant in equation (18) (note that $L \to \infty$):

$$\lim_{N\to\infty} s_k(h,N,x) = \frac{\sin(\pi(x-kh)/h)}{\pi(x-kh)/h)} \equiv S_k(h,x). \tag{22}$$

This property justifies the name of LSF.

Figure 2 compares two LSF for $N = 40$ and $L = 1$ with the corresponding sinc functions. Differences between both kind of functions are appreciable only in the right plot, corresponding to $k = 19$. In this case, the LSF is slightly larger than unity at the peak and its oscillations die out faster.

[3] We thank one of the referees for pointing out this relation.

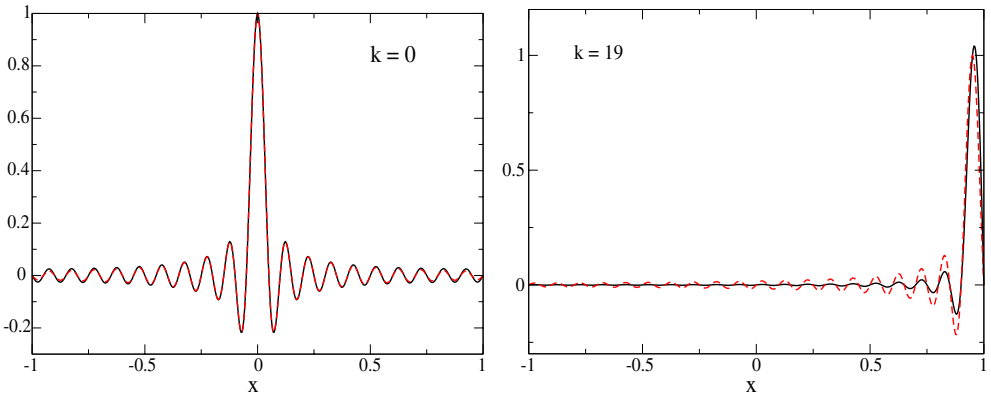

Figure 2. Comparison between the sinc functions (dashed line) and the little sinc functions (solid line) corresponding to $N = 40$.

The LSF share some properties with the sinc functions, for example, we can approximate a function $f(x)$ on the interval $(-L, L)$ as

$$f(x) \approx \sum_{k=-N/2+1}^{N/2-1} f(x_k) s_k(h, N, x), \tag{23}$$

where $x_k \equiv kh$.

To understand this point we can use the definition of $s_k(h, N, x)$ in terms of the completeness relation and write equation (23) as

$$f(x) \approx \sum_{n=1}^{N} \left(h \sum_{k=-N/2+1}^{N/2-1} f(x_k)\psi_n(x_k) \right) \psi_n(x). \tag{24}$$

In the limit $N \to \infty$ (i.e. $h \to 0$) the term in the parenthesis reduces to the integral $\int_{-L}^{+L} f(y)\psi_n(y)\mathrm{d}y$ and the relation becomes exact

$$f(x) = \sum_{n=1}^{N} \left[\int_{-L}^{+L} f(y)\psi_n(y)\,\mathrm{d}y \right] \psi_n(x).$$

Similarly, one can express the derivatives of LSF in terms of LSF as

$$\frac{\mathrm{d}s_k(h, N, x)}{\mathrm{d}x} \approx \sum_j \left. \frac{\mathrm{d}s_k(h, N, x)}{\mathrm{d}x} \right|_{x=x_j} s_j(h, N, x) \equiv \sum_j c_{kj}^{(1)} s_j(h, N, x) \tag{25}$$

$$\frac{\mathrm{d}^2 s_k(h, N, x)}{\mathrm{d}x^2} \approx \sum_j \left. \frac{\mathrm{d}^2 s_k(h, N, x)}{\mathrm{d}x^2} \right|_{x=x_j} s_j(h, N, x) \equiv \sum_j c_{kj}^{(2)} s_j(h, N, x), \tag{26}$$

where the $c_{kj}^{(r)}$ are the counterpart of the coefficients shown above for the sinc functions.

An explicit calculation yields

$$c_{jj}^{(1)} = \frac{\pi}{4L} \tan\left(\frac{j\pi}{N} \right) \tag{27}$$

$$c_{kj}^{(1)} = (-1)^{k-j}\frac{\pi}{4L}\left(\cot\left(\frac{(j-k)\pi}{2N}\right) + \tan\left(\frac{(j+k)\pi}{2N}\right)\right) \tag{28}$$

and

$$c_{jj}^{(2)} = -\frac{\pi^2}{24L^2}\left(1 + 2N^2 - 3\sec^2\left(\frac{j\pi}{N}\right)\right) \tag{29}$$

$$c_{kj}^{(2)} = -(-1)^{j-k}\frac{\pi^2}{8L^2}\frac{\cos\left(\frac{j\pi}{N}\right)\cos\left(\frac{k\pi}{N}\right)}{\cos^2\left(\frac{\pi}{2N}(j+k)\right)\sin^2\left(\frac{\pi}{2N}(j-k)\right)}. \tag{30}$$

Because of equation (22) these matrices reduce to the usual sinc expressions given in the preceding section when $N \to \infty$.

It is straightforward to generalize equation (18), defined in $(-L, L)$, to an arbitrary interval (a, b):

$$\tilde{s}_k(h, N, x) \equiv s_k\left(h, N, x - \frac{a+b}{2}\right). \tag{31}$$

In this case, the points of the grid are given by

$$x_k = \frac{2Lk}{N-2} + \frac{a+b}{2}. \tag{32}$$

In order to apply sinc collocation on a finite interval one commonly maps the real line onto $[a, b]$ [10] by means of the conformal transformation

$$\phi(z) = \log\left(\frac{z-a}{b-z}\right). \tag{33}$$

This map carries the eye-shaped region

$$D_E = \left\{z = x + \mathrm{i}y : \left|\arg\left(\frac{z-a}{b-z}\right)\right| < d \leqslant \frac{\pi}{2}\right\} \tag{34}$$

onto the infinite strip

$$D_S = \left\{w = u + \mathrm{i}v : |v| < d \leqslant \frac{\pi}{2}\right\}. \tag{35}$$

Under the inverse transformation $z = \phi^{-1}(w)$ the points of the uniform grid on the real axis, given by $u_k = kh$, are mapped onto the non-uniform grid defined by the points $\overline{x}_k = (a + b\,\mathrm{e}^{kh})/(1 + \mathrm{e}^{kh})$.

In this case, the sinc functions are mapped onto

$$\overline{S}_k(h, x) \equiv \frac{\sin(\pi(\phi(x) - kh)/h)}{\pi(\phi(x) - kh)/h}, \tag{36}$$

which equals unity at $x = \overline{x}_k$. Consequently, it is possible to approximate a function in the interval (a, b) as

$$f(x) \approx \overline{f}(x) = \sum_{k=-N}^{+N} f(\overline{x}_k)\overline{S}_k(h, x). \tag{37}$$

The LSF, on the other hand, apply directly to a finite domain. We can test the performance of the LSF on an example selected from [14]:

$$f(x) = 2x^2 + x - 3x^3, \tag{38}$$

where $0 \leqslant x \leqslant 1$ and $f(0) = f(1) = 0$. Figure 3 compares the logarithmic error $\Delta(x) \equiv \log_{10}|f(x) - \overline{f}(x)|$ for both kind of functions. The solid curve corresponds to 21

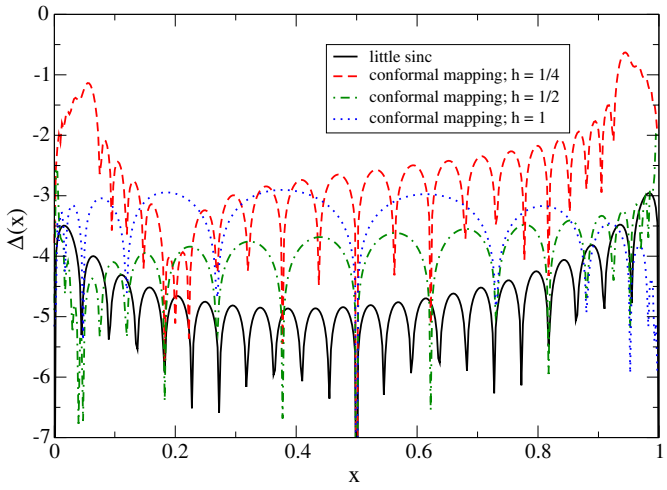

Figure 3. Error in the interpolation of $f(x)$ in equation (38) using 21 functions.

LSF, whereas the other three curves correspond to the same number of conformally mapped sinc functions with spacing $h = 1/4, 1/2$ and 1, respectively. The LSF produce smaller errors and offer the advantage of a uniform grid.

Stenger originally introduced sinc methods for the numerical solution of differential equations [11]. Sinc-Galerkin and sinc collocation methods are particularly useful in dealing with these problems since they converge exponentially even in the presence of boundary singularities. It is not our purpose to generalize all the known mathematical results from the sinc functions to the LSF; however, we assume that both kind of functions share similar properties and simply compare our LSF results with those provided by the conformally mapped sinc functions.

We consider example 4.1 of [13], that is to say, the inhomogeneous differential equation (note a typo in [13], where the term $69x$ should read $62x$)

$$-u''(x) + u'(x) + u(x) = \left(\tfrac{4}{25}\right)^2 (x^4 - 2x^3 - 29x^2 + 62x + 38), \tag{39}$$

with the boundary conditions $u(-1) = u(4) = 0$. The exact solution to this equation is

$$u_{\text{eact}}(x) = \left(\tfrac{4}{25}\right)^2 (x+1)^2(x-4)^2. \tag{40}$$

We look for a numerical solution in terms of our LSF as

$$u_{\text{LS}}(x) = \sum_{k=-N/2+1}^{N/2-1} u_k s_k(h, N, x - 3/2), \tag{41}$$

where the coordinate shift $(x - 3/2)$ follows from equation (31) with $a = -1, b = 4$ and $2L = b - a$. The coefficients u_k are obtained by substitution of the ansatz (41) into equation (39).

Figure 4 shows global and local errors defined, respectively, as

$$\begin{aligned} \Xi_G(N) &\equiv \log_{10}\left|\int_{-1}^{4} (u_{\text{exact}}(x) - u_{\text{LS}}(x))^2\,\mathrm{d}x\right| \\ &= \log_{10}\left|\int_{-1}^{4} u^2_{\text{exact}}(x)\,\mathrm{d}x - h\sum_{k=-N/2+1}^{N/2-1} u_k^2\right| \end{aligned} \tag{42}$$

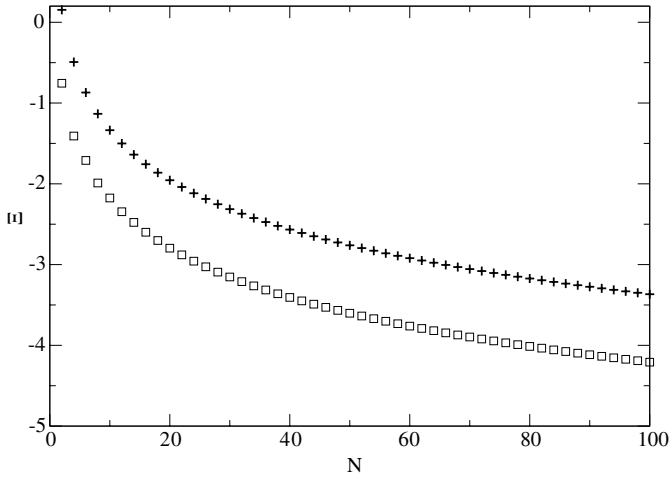

Figure 4. Global (crosses) and local (square) errors (42) and (43), respectively, for the solution of equation (39) in terms of $(N-1)$ LSF.

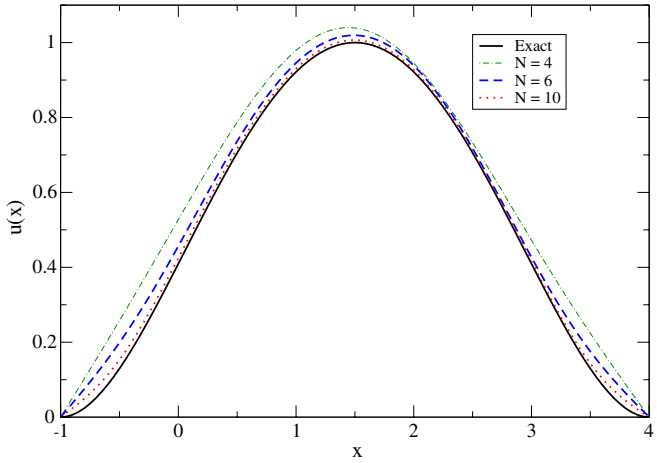

Figure 5. Comparison between the exact solution $u_{\text{exact}}(x)$ (solid line) and the approximations obtained using LSF with $N = 4, 6, 10$.

$$\Xi_L(N) \equiv \log_{10}|u_{\text{exact}}(3/2) - u_{\text{LS}}(3/2)|. \tag{43}$$

Note that at large N the errors appear to decay exponentially. Unlike [13] no domain decomposition was required to solve this problem. Figure 5 compares several approximations $u_{\text{LS}}(x)$ with the exact solution $u_{\text{exact}}(x)$.

4. The Schrödinger equation

As mentioned in the introduction, sinc collocation methods have been used to obtain accurate numerical solutions to the Schrödinger equation. In this section, we wish to extend the variational approach and the results of [17] to our LSF and generalize the variational method

to include potentials with both bound and unbound states. To simplify this presentation we begin with potentials supporting only bound states.

4.1. Potentials that support only bound states

We consider the one-dimensional Schrödinger equation

$$-\frac{\hbar^2}{2m}\frac{\mathrm{d}^2\psi_n(x)}{\mathrm{d}x^2} + V(x)\psi_n(x) = E_n\psi_n(x) \tag{44}$$

on an interval (a, b), which can be either finite or infinite. The wavefunctions $\psi_n(x)$ obey the boundary conditions $\psi_n(a) = \psi_n(b) = 0$, which grant that there will be only bound states.

If we express the wavefunctions in terms of our LSF, then equations (23), (26) and (30) allow one to derive the following matrix representation of the Hamiltonian operator

$$H_{kl} = -\frac{\hbar^2}{2m}c_{kl}^{(2)} + \delta_{kl}V(kh). \tag{45}$$

This equation is similar to equation (8) of [17], except for the form of the matrix $\mathbf{c}^{(2)}$. Once the spacing h of the grid is fixed, then the $(N \times N)$ matrix $\mathbf{H}_N$ for a manifold of N LSF can be diagonalized. In this way, one obtains an approximation to the first N eigenvalues and wavefunctions of the Schrödinger equation (44).

The precision of the approximate results obtained by diagonalization of the Hamiltonian matrix (45) depends crucially on both the number of LSF as well as on the grid spacing. In fact, although a small spacing can help to increase the resolution, if the number of the sinc functions is not large enough, the approximation will not be able to grasp the natural scale of the problem and the overall precision will be poor. On the other hand, a large spacing will certainly provide poor results, because the details of the problem will not be resolved. Based on these observations it is easy to convince oneself that there must exist an optimal spacing for a given number of functions. Finding this optimal spacing will allow one to reach sufficiently accurate results with a relatively small number of grid points.

It was found earlier [17] that an optimal spacing can be obtained by straightforward application of the PMS to the trace of the $(N \times N)$ Hamiltonian matrix $\mathcal{T}_N(h) = Tr\,[\mathbf{H}_N]$. In fact, given that the trace of a Hamiltonian is invariant under unitary transformations, and that in the limit $h \to 0$ it will be independent of h, then it is reasonable to obtain such optimal spacing from the solution of the equation

$$\frac{\mathrm{d}}{\mathrm{d}h}\mathcal{T}_N(h) = 0. \tag{46}$$

Such property was invoked earlier when using a basis of harmonic-oscillator wavefunctions depending on an arbitrary scale parameter [20]. Therefore, the optimal value of h is found by numerically solving a single algebraic equation, a modest computational task. In other words, the interval length L appearing in LSF is treated as a variational parameter.

Strictly speaking, since equations (23) and (45) are only approximate, small violations of the variational principle can be expected. These violations, however, will be arbitrarily small as the number of points in the grid is increased: this explains the success of the approach of [17].

Schwartz has given an expression for the optimal grid spacing, derived from the behaviour of the wavefunction at large distances [2]. In what follows we compare Schwartz's expressions [2] for the polynomial potentials $V(x) = x^s/s$ with the result provided by the application of the PMS, discussed above.

We consider the kinetic and potential contributions to the trace $\mathcal{T}_N$ separately. The former is given by

$$\mathcal{K}_N = -\frac{\hbar^2}{2m}\sum_{k=-N/2+1}^{N/2-1} c_{kk}^{(2)} = \frac{\hbar^2\pi^2}{48mL^2}\sum_{k=-N/2+1}^{N/2-1}\left(1+2N^2-3\sec^2\left(\frac{k\pi}{N}\right)\right).$$

For large N we can expand the secant in the sum around $N/2$ and $-N/2$, where this term dominates and then perform the sum. Following this procedure one obtains a quite accurate approximation

$$\mathcal{K}_N \approx \frac{\hbar^2\pi^2}{24mL^2}\left[-1+N^2(N-1)-\frac{3N^2}{\pi^2}H^{(2)}_{\frac{N}{2}-1}\right] \approx \frac{\hbar^2\pi^2}{24mL^2}\left(N^3-\frac{3N^2}{2}-1\right),$$

where $H_n^{(s)} \equiv \sum_{k=1}^{n} 1/k^s$ is the generalized harmonic number. Note that $\lim_{N\to\infty} H^{(2)}_{\frac{N}{2}-1} = \zeta(2) = \pi^2/6$.

The contribution of the potential to the trace for s even is

$$\mathcal{V}_N = \sum_{k=-N/2+1}^{N/2-1} V(x_k) \approx \frac{1}{h}\int_{-L}^{+L} V(x)\,\mathrm{d}x = \frac{NL^s}{s(s+1)}. \tag{47}$$

Note the different dependence of the kinetic and potential terms upon the length parameter L. The PMS yields the optimal value

$$L_{\mathrm{PMS}} \approx \left[\frac{\hbar^2\pi^2}{24mN}(s+1)(2N^3-3N^2-2)\right]^{1/(s+2)} \tag{48}$$

from which it follows that

$$h_{\mathrm{PMS}} = \frac{2L_{\mathrm{PMS}}}{N} \approx \frac{2}{N}\left[\frac{\hbar^2\pi^2}{24mN}(s+1)(2N^3-3N^2-2)\right]^{1/(s+2)} \tag{49}$$

exhibits the same N-dependence as Schwartz's equation (18) [2] for the chosen potentials. Note that the physical solution of the Schrödinger equation with a potential $V(x) = x^s/s$ behaves asymptotically as $\psi(x) \approx \mathrm{e}^{-cx^p}$ where $p = s/2+1$, for $|x| \gg 1$. We have also verified numerically that our analytical expression describes quite accurately the true behaviour of h_{PMS} even for moderate values of N.

In particular, after setting $\hbar = m = 1$ and $s = 2$, which corresponds to the harmonic oscillator, our formula reduces to

$$h_{\mathrm{PMS}} \approx \sqrt{\frac{2\pi}{N}}\left[1-\frac{3}{2N}-\frac{1}{N^3}\right]^{1/4} \approx \sqrt{\frac{2\pi}{N}}, \tag{50}$$

which is precisely Schwartz's equation (22) [2] after identifying $N = 2N_{\mathrm{Schwartz}}$. It is quite suggestive that h_{PMS} is similar to the value of h obtained by Schwartz from the asymptotic behaviour of the wavefunction. In the case of the quartic oscillator ($s = 4$) we obtain

$$h_{\mathrm{PMS}} \approx \left[\frac{80\pi^2}{3N^4}\right]^{1/6}\left[1-\frac{3}{2N}-\frac{1}{N^3}\right]^{1/6} \approx 2.5315N^{-2/3}, \tag{51}$$

that is quite close to Schwartz's equation (23)

$$h_{\mathrm{Schwartz}} = \left(\frac{2^{5/6}\pi}{N_{\mathrm{Schwartz}}^2}\right)^{1/3} \approx 1.78N_{\mathrm{Schwartz}}^{-2/3} = 2.8256N^{-2/3}. \tag{52}$$

Using our formula for the ground state we have obtained an error that decays exponentially as $\Xi \approx \mathrm{e}^{-0.95N}$, compared with the $\Xi \approx \mathrm{e}^{-1.32N}$ of equation (25) of [2]. Note that while

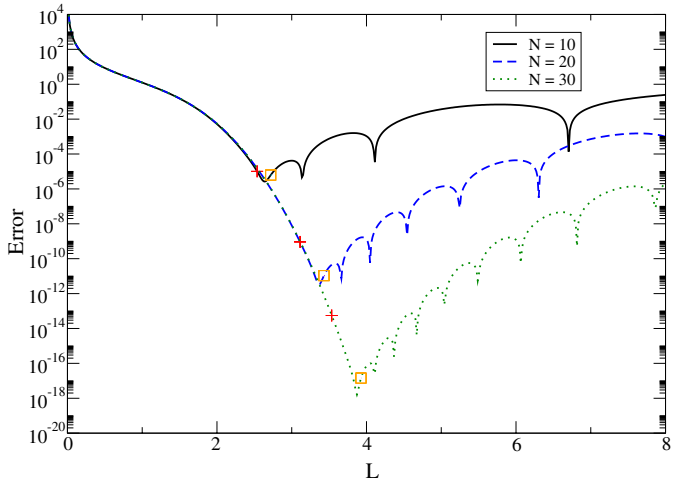

Figure 6. Error in the ground-state energy of the potential (53) using $N = 10$, 20 and 30, as a function of the parameter L. The plus and square symbols correspond to the PMS and modified PMS conditions, respectively.

Schwartz's result is limited to a specific class of potentials the extension of the PMS to more general potential poses no problem.

As a further test of our method we apply it to the first example in [7], i.e the harmonic oscillator with $\hbar = 1$, $m = 1/2$ and $\omega = 2$. Using a Cartesian mesh, Baye and Heenen reported errors smaller than 10^{-3} for the first three eigenvalues and $N = 10$. On the other hand, our LSF approach with $N = 10$ (which corresponds to 9 sinc functions), and a grid spacing optimized according to equation (46), yields errors $(E^{\text{exact}} - E^{\text{approx}})$ of -4.86×10^{-6}, 1.2×10^{-4} and -1.6×10^{-3} for the same cases.

The authors of [7] also observe that for $N = 50$, the high eigenvalues become very sensitive to the value of h, and that the variation of the 30th eigenvalue with respect to h presents a marked minimum around $h = 0.35$. It is remarkable that the PMS condition for $N = 50$ yields $L_{\text{PMS}} = 8.93$, corresponding to $h_{\text{PMS}} = 2L_{\text{PMS}}/N \approx 0.357$, which is extremely close to the value quoted by Baye and Heenen. It is worth noting that while the optimal value of h quoted by Baye and Heenen is the result of an empirical observation, the almost identical value of h given by the PMS is just the numerical solution of the algebraic equation (46), which requires a negligible computer time.

As a second example of application of the PMS to the LSF collocation method we consider the anharmonic potential

$$V(x) = x^2 + x^4 \tag{53}$$

and assume that $\hbar = 1$ and $m = 1/2$ in the Schrödinger equation. This example was also studied by Baye and Heenen [7] who obtained the optimal values $h = 0.55$ for $N = 10$, and $h = 0.2$ for $N = 50$ using a Cartesian mesh, which is somehow related to the LSF. Figure 6 shows the error $\left|E_0^{\text{exact}} - E_0^{\text{approx}}\right|$ as a function of the parameter L for three different values of N (remember that the number of LSF in the expansion is $N - 1$). The plus symbols in the plot correspond to the predictions of the PMS condition, which generally fall close to the minimum of the curve, while the square symbols correspond to the solutions of a sort of empirical PMS

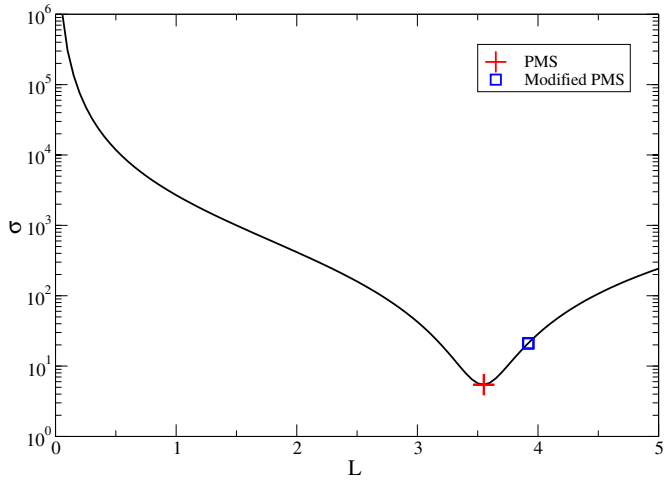

Figure 7. Global error $\sigma \equiv \sum_{n=0}^{18} |E_n^{(20)} - E_n^{(60)}|$ for the potential $V(x) = x^4/4$.

condition, obtained by minimizing the modified trace

$$\tilde{\mathcal{T}}_N(h) = \mathcal{T}_N(h) - \frac{N-2}{2N} \sum_k V(x_k). \tag{54}$$

with respect to L. We remark that this condition is *empirical* and specifically Taylored for the potential (53). The better behaviour of the modified PMS condition for just one state (as in figure 6) should not confuse the reader. It must be kept in mind that the PMS minimizes a sort of global error for all the states in the chosen manifold. In order to appreciate this point clearly, figure 7 shows the global error $\sigma = \sum_{n=0}^{N-1} \left| E_n^{(N)} - E_n^{(\text{exact})} \right|$ as a function of L for the potential $x^4/4$ and $N = 20$. Note that in this case the PMS condition yields the minimal error. The exact energies $E_n^{(\text{exact})}$ were simply chosen to be those given by the method at higher order: $E_n^{(60)}$.

The accuracy of the present calculations is greater than that obtained earlier for the same problem [7], where the authors report errors of the order of 10^{-5} and 10^{-12} for $N = 10$ and $N = 50$, respectively. Figure 6 shows that the curves with different values of N overlap in the region of small L, which suggests that the approach may not be taking into account the large-L region correctly.

4.2. Potentials supporting bound and unbound states

In what follows we try and show that the LSF are suitable for the treatment of bound states of potentials that also support unbound states. The application of the PMS condition to potentials with both discrete and continuous spectra is not straightforward. The potentials treated in the preceding section increase with the coordinate and therefore the matrix representation of those potentials increase with L. Since the matrix representation of the kinetic energy decreases with L then there is a minimum in the trace of the Hamiltonian matrix and the PMS gives a balance between the traces of both contributions. That minimum provides the natural length scale for the application of the method. If the potential energy tends to a finite constant value as the coordinate increases, then there may not be a minimum and the PMS will not yield the length scale for the application of the present approach.

In order to overcome that problem we substitute a potential $\tilde{V}(x)$ into the Schrödinger equation that behaves exactly as the original potential $V(x)$ in the relevant coordinate region and increases to infinity at large distances. The error introduced by such potential substitute will be negligible if the difference between the original and substitute potentials is appreciable only where the wavefunctions are expected to be vanishing small. This substitution removes the continuous spectrum but should not affect the discrete one too much. The advantage is that we are thus able to apply the PMS condition exactly as in the preceding subsection.

Note that the substitute potential is introduced with the sole purpose of obtaining the length scale and that we diagonalize the correct Hamiltonian matrix.

We illustrate our procedure on the Morse potential already treated earlier by means of the Lagrange mesh method [8]:

$$V(r) = D[\mathrm{e}^{-2a(r-r_e)} - 2\,\mathrm{e}^{-a(r-r_e)}], \tag{55}$$

where $D = 0.102\,62$, $r_e = 2$, $a = 0.72$, $2m = 1836$ and $\hbar = 1$. In the case of states with nonzero angular momentum we should add the centrifugal potential $\frac{\hbar^2 l(l+1)}{2mr^2}$, $l = 0, 1, 2, \ldots$.

The substitute potential $\tilde{V}(r)$ is arbitrary; we can, for example, choose it to be the Taylor expansion of $V(r)$ around a given point, truncated at a sufficiently large order so that it is accurate enough at small r, and at the same time satisfies $\lim_{r\to\infty} \tilde{V}(r) = +\infty$. The expansion of the potential about a point close to its minimum gives rise to a right branch that increases sharply at moderate values of r. For this reason it is preferable to choose a point far to the right of the minimum in order to obtain an auxiliary potential $\tilde{V}(r)$ that accounts better for the actual scale of the problem. The resulting auxiliary potential may be less accurate to the left of the minimum but this inaccuracy does not affect the choice of the optimum length parameter. For example, in the present particular case we can choose

$$\tilde{V}(r) = \sum_{n=0}^{20} \frac{1}{n!} \left.\frac{\mathrm{d}^n V}{\mathrm{d}r^n}\right|_{r=10} (r-10)^n. \tag{56}$$

Another difficulty to take into consideration is that our LSF are defined in $(-L, L)$, whereas the radial coordinate is defined in $(0, +\infty)$. The obvious solution to this apparent problem would be to follow Baye's strategy [3], where the left boundary of the interval is 0; on the other hand, such choice would be equivalent to a shift by a proper amount of the potential, thus bringing the boundary condition on the left point to coincide with the left point of the LSF. Despite its simplicity, this procedure is not optimal and generally does not provide the best results. We have found out that a more convenient strategy consists of keeping our LSF unchanged and shifting the coordinate by given amount as $V(r) \to V(r + \overline{r})$, where $\overline{r}$ is typically close to the minimum of the potential (the same shift should be applied to the centrifugal energy when $l > 0$). The PMS applied to the shifted Hamiltonian will thus provide the optimal scale for the application of the LSF collocation method.

One advantage of that procedure is that it maximizes the sampling of the classically allowed region, where the bound state wavefunctions exhibit marked nonzero contributions. Of course, in order to take into account the boundary condition at $r = 0$, the PMS length scale has to be smaller than $\overline{r}$.

Table 1 shows the errors $\epsilon_n \equiv E_n^{\mathrm{approx}} - E_n^{\mathrm{exact}}$ for the s, p and d states of the Morse potential with $n = 0$ and $n = 5$. It compares the present results with those of Baye *et al* [8]. The last column of table 1 displays the PMS optimal values of the grid spacing, where we have chosen $\overline{r} = 3$.

Figure 8 shows the local error $\eta_N(x) = |\psi^{(N)}(x) - \psi^{(80)}(x)|$ for the ground state of the Morse potential and approximations $N = 20$ and $N = 40$. We assume that the approximation of order $N = 80$ is sufficiently close to the exact wavefunction. Our results are more

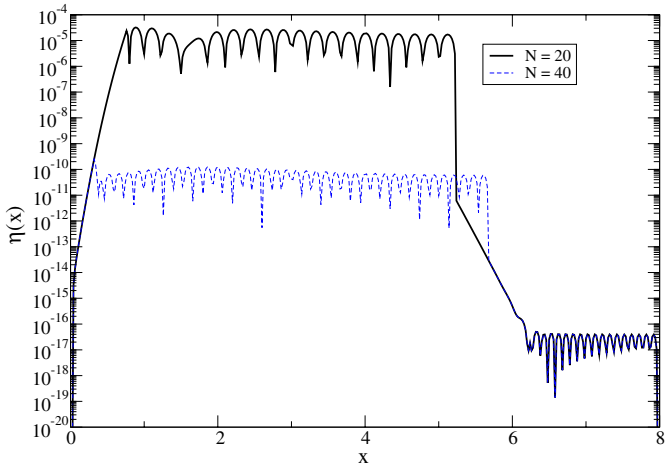

Figure 8. Error $\eta_N(x) = |\psi^{(N)}(x) - \psi^{(80)}(x)|$ as a function of x for the ground state of the Morse potential.

Table 1. Errors $\epsilon_n \equiv E_n^{\text{approx}} - E_n^{\text{exact}}$ for some states of the Morse potential. Powers of ten are indicated between square brackets. E_n^{exact} is approximated with the energy calculated for $N = 80$.

l	n	N	[8]	PMS	h_{PMS}
0	0	20	3.8[−7]	−3.3[−10]	0.223
		40	<1[−14]	1.8[−20]	0.134
	5	20	4.0[−3]	2.1[−6]	0.223
		40	1.1[−9]	2.5[−14]	0.134
1	0	20	4.1[−7]	−3.6[−10]	0.223
		40	<1[−14]	−1.6[−20]	0.134
	5	20	4.4[−3]	1.5[−6]	0.223
		40	1.1[−9]	2.9[−14]	0.134
2	0	20	4.5[−7]	−4.1[−10]	0.223
		40	<1[−14]	1.2[−20]	0.134
	5	20	4.7[−3]	2.0[−7]	0.223
		40	1.1[−9]	3.9[−14]	0.134

accurate than those of Baye *et al* [8] who essentially considered the average of $\eta(x)$ over a chosen region. The sharp drop of the error beyond a certain value of r, clearly noticeable in figure 8, is due to the fact that our LSF reproduce the wavefunction only in a finite region outside which $\eta(x)$ is incorrectly given by the value of $|\psi^{(80)}(x)|$. It is worth noting that $\eta_N(x)$ is almost uniform in the region covered by the LSF.

We have also applied our method to the one-dimensional Morse potential considered by Wei [21]:

$$V(x) = D[\mathrm{e}^{-2\alpha x} - 2\,\mathrm{e}^{-\alpha x} + 1], \tag{57}$$

where $-\infty < x < \infty$, $D = 0.0224$, $\alpha = 0.9374$, $m = 119\,406$ and $\hbar = 1$. This problem can be solved exactly and the energies are given by [22]

$$E_n = \hbar\omega\left[n + \frac{1}{2} - \frac{\hbar\omega}{4D}\left(n + \frac{1}{2}\right)^2\right], \tag{58}$$

where $\omega = \sqrt{2D/m}\alpha$. As before we can improve our results by conveniently shifting the potential on the x-axis from $V(x)$ to $V(x+\overline{x})$. When $N = 20$ and assuming $\overline{x} = 0$ we have found that the first-excited-state eigenvalue is reproduced with an accuracy of about 8×10^{-14}, which is even better than the accuracy obtained by Wei with $N = 64$. (Note that table 1 of [21] omits the ground state of the model.) When $N = 40$ the error of our method is just 8.1×10^{-21} for the ground state.

5. Conclusions

We have discussed a class of orthogonal functions, which share some properties with the usual sinc functions, but which are defined on finite intervals. In this paper, we have referred to these functions as 'little sinc functions' (LSF). We have shown that the LSF collocation method provides accurate approximations for a wide class of problems when it is supplemented by the principle of minimal sensitivity (PMS) that selects an optimal grid spacing. In particular, we have applied the LSF to the solution of the Schrödinger equation with only bound states and with mixed discrete and continuous spectra. We have chosen benchmark models treated earlier by other authors and in all the cases we obtained more accurate results. It seems that the LSF collocation method is an interesting alternative algorithm for solving many mathematical and physical problems.

Acknowledgment

FMF thanks the University of Colima for support through project PIFI 3.2.

References

[1] Meyer R 1970 Trigonometric interpolation method for one-dimensional quantum-mechanical problems *J. Chem. Phys.* **52** 2053–9
[2] Schwartz C 1985 High-accuracy approximation technique for analytic functions *J. Math. Phys.* **26** 411–5
[3] Baye D 1995 Constant-step Lagrange meshes for central potentials *J. Phys. B: At. Mol. Opt. Phys.* **28** 4399–412
[4] Mostofi A A, Haynes P D, Skylaris C K and Payne M C 2003 Preconditioned iterative minimization for linear-scaling electronic structure calculations *J. Chem. Phys.* **119** 8842–8
[5] Amore P 2007 Alternative representation for nonlocal operators and path integrals *Phys. Rev.* A **75** 032111
[6] Colbert D T and Miller W H 1992 A novel discrete variable representation for quantum mechanical reactive scattering via the *S*-matrix Kohn method *J. Chem. Phys.* **96** 1982–91
[7] Baye D and Heenen P H 1986 Generalised meshes for quantum mechanical problems *J. Phys. A: Math. Gen.* 2041–59
[8] Baye D, Hesse M and Vincke M 2002 The unexplained accuracy of the Lagrange-mesh method *Phys. Rev.* E **65** 026701
[9] Koures V G and Harris F E 1996 Sinc collocation in quantum chemistry: solving the planar coulomb Schrödinger equation *Int. J. Quantum Chem.* **30** 1311
[10] Stenger F 1993 *Numerical Methods Based on Sinc and Analytic Functions* (New York: Springer)
[11] Stenger F 1979 A sinc-Galerkin method of solution of boundary value problems *Math. Comput.* **33** 85–109
[12] Morlet A C 1995 Convergence of the sinc method for a fourth-order ordinary differential equation with an application *SIAM J. Numer. Anal.* **32** 1475–503
[13] Lybeck N J and Bowers K L 1996 Sinc methods for domain decomposition *Appl. Math. Comput.* **75** 13–41
[14] Narashiman S, Majdalani J and Stenger F 2002 A first step in applying the sinc collocation method to the nonlinear Navier–Stokes equations *Numer. Heat Transfer* **41** 447–62
[15] Easther R, Guralnik G and Hahn S 2000 Fast evaluation of Feynman diagrams *Phys. Rev.* D **61** 125001
[16] Revelli R and Ridolfi L 2003 Sinc collocation–interpolation method for the simulation of nonlinear waves *Comput. Math. Appl.* **46** 1443–53
[17] Amore P 2006 A variational sinc collocation method for strong coupling problems *J. Phys. A: Math. Gen.* **39** L349–55

[18] Stevenson P M 1981 Optimized perturbation theory *Phys. Rev.* D **23** 2916
[19] Abramowitz M and Stegun I A 1965 *Handbook of Mathematical Functions* (New York: Dover)
[20] Amore P, Aranda A, Jones H F and Fernández F M 2005 A new approximation method for time independent problems in quantum mechanics *Phys. Lett.* A **340** 87–93
[21] Wei G W 2000 Solving quantum eigenvalue problems by discrete singular convolution *J. Phys. B: At. Mol. Opt. Phys.* **33** 343–52
[22] Fernández F M 2001 *Introduction to Perturbation Theory in Quantum Mechanics* (Boca Raton, FL: CRC Press)